On fuzzy modelling of dynamic track behaviour

(article starts on next page)

Railway Engineering Science
https://doi.org/10.1007/s40534-024-00370-4

On fuzzy modelling of dynamic track behaviour

Katja Stampka[1] · Vincent Radmann[1] · Jannik Theyssen[2] · Ennes Sarradj[1]

Received: 23 May 2024 / Revised: 19 November 2024 / Accepted: 24 November 2024

Abstract
Rolling noise is an important source of railway noise and depends also on the dynamic behaviour of a railway track. This is characterized by the point or transfer mobility and the track decay rate, which depend on a number of track parameters. One possible reason for deviations between simulated and measured results for the dynamic track behaviour is the uncertainty of the value of some track parameters used as input for the simulation. This in turn results in an uncertainty in the simulation results. In this contribution, it is proposed to use the general transformation method to assess a uncertainty band for the results. Most relevant input parameters for determining the point input mobility and the track decay rate for a ballasted track are analysed with regard to the uncertainties and for the value of each an interval is determined. Then, the general transformation method is applied to four different simulation methods, working both in the frequency and time domains. For one example track, the resulting uncertainty bands are compared to one dataset with measurements for the point mobility and the track decay rate. In addition, a sensitivity analysis is performed to determine the parameters that significantly influence the overall result. While all four simulation methods produce broad uncertainty bands for the results, none did match the measured results for the point mobility and the track decay rate over the entire frequency range considered. Besides the large influence of the uncertain pad stiffness, it turned out that the rail wear is also a significant source of uncertainty of the results. Overall, it is demonstrated that the proposed approach allows assessing the influence of uncertain input parameters in detail.

Keywords Dynamic track behaviour · Uncertainty · General transformation method · Track decay rate · Rolling noise

1 Introduction

Railway noise is composed of aggregate, aerodynamic, and rolling noise [1]. Rolling noise is an important sound source, as it is the dominant sound source over a wide range of train speeds. It is generated by the interactions of the irregularities found on both the rail and the wheel tread on contact and by parametric excitation at most track types, resulting from the variable stiffness of the rail support along the track. Both wheel and the rail radiate this noise as airborne sound. The decay of the rail vibration along the track influences the intensity of the airborne sound emitted by the rail. The track decay rate (TDR) can be determined as a measure of this decay [2]. In addition to this, the dynamic response of the track can be characterized via the point input mobility [1].

Numerous models for predicting track vibration are discussed in a recent review article [3]. Measured data and simulation results are frequently compared to assess the quality of a model. However, it must be considered that deviations between measured values and simulations, in addition to measurement errors, are caused by model uncertainties or incorrectly specified parameters. Even with a high-quality model, inadequate simulation results can be produced if the input parameters are not specified appropriately.

For the simulation of the track, several parameters describing the rail itself, as well as the superstructure, are required. However, obtaining the exact parameters is sometimes difficult. On the one hand, the parameters change over time, for example, due to weather or wear [4, 5]. On the other hand, these parameters vary considerably depending on the measurement method or installation situation. Already Knothe and Grassie [6] concluded that the parameters of the pads and ballast cannot always be specified with the accuracy needed for reliable simulations.

✉ Ennes Sarradj
ennes.sarradj@tu-berlin.de

1 Engineering Acoustics, Technische Universität Berlin, Einsteinufer 25, 10587 Berlin, Germany

2 Division of Applied Acoustics, Chalmers University of Technology, Sven Hultins Gata 6, 41258 Gothenburg, Sweden

Published online: 09 May 2025

To determine the unknown parameters as accurately as possible, parameters are often approximated by matching them with existing measurements using curve-fitting methods [7–9]. However, the accuracy of this procedure is challenging to quantify. It depends on the model used to fit the curve as well as on the quality of the measurement data. Therefore, the parameter values still must be assumed to be somewhat inaccurate. To the best of the authors' knowledge, other solutions for handling uncertain input parameters for rolling noise simulations are unavailable in the literature. This is true however not only in this context but appears frequently in the context of simulations in general.

The general transformation method (GTM) addresses the issue of uncertain input parameter mentioned above by applying fuzzy arithmetic. Hanss [10, 11] and others [12, 13] introduce this method for various non-acoustic applications. Seidel et al. [14] use it in an acoustic context for vibro-acoustic research of aircraft structures. With this method, the parameters are assumed to be fuzzy and are not specified by a single value. Thus, it is feasible to establish fuzzy results, which can be understood as the possible range of the simulation results for the uncertainty of the given input parameters. Furthermore, the influence of a single fuzzy parameter can be evaluated by a sensitivity analysis. Such analysis can estimate the influence of each fuzzy parameter on the simulation result as a function of frequency [11]. In this way, parameters that considerably influence the final results can be identified.

The current work introduces the GTM as an example for determining the point input mobility and the TDR of a ballasted track. Four different simulation methods were chosen to showcase the application of fuzzy arithmetic to rail vibration simulations. They include methods that work in the frequency domain, as well as such that work in the time domain. Moreover, the track is modelled with varying degrees of precision. Fuzzy parameters are identified through a comprehensive literature review, and a value range is defined for each of these parameters. For the four simulation methods, fuzzy results are calculated for predicting both the point input mobility mid-span and the TDR with the hammer impact method [2]. The fuzzy results are analysed and then compared with measured data. Additionally, a comprehensive sensitivity analysis is conducted to quantify the influence of specific input parameters.

The remainder of the paper is structured as follows: First, the simulation methods and the fuzzy arithmetic are introduced. Then, the track parameters and their uncertainty are reviewed, and the implementation of GTM for the analysis is discussed. The fuzzy results and a sensitivity analysis are presented. Finally, a comparison of the four models is used for a discussion of the results.

2 Simulation methods

There are various methods in the literature for calculating rail vibrations with different advantages and disadvantages. A comprehensive overview of the different methods is given in [3]. Four different simulation methods are used in the present investigation of a ballasted track. The first is a time domain method based on the finite difference method (FDM) [15]. A Green's function method (GFM) [9] is also used to calculate the track decay rate in the frequency domain, which can also provide results in the time domain. These are compared with two frequency domain models: one, in which the track support is modelled by a point reaction force (PFM) described by Heckl [16, 17] and one, in which the waveguide finite element method (2.5D FEM) is used [18–20]. An overview of the basic properties of the four methods used is given in Table 1.

The literature offers many ways of modelling a ballasted track [3]. In this case, a two-layer model is used; see Fig. 1. Depending on the simulation method, the rail is either approximated as a beam (FDM, GFM, and PFM) or described by the rail cross-section geometry (2.5D FEM).

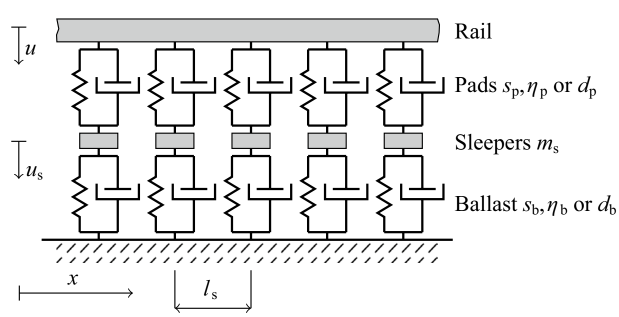

Fig. 1 Two-layer model of a ballasted track

Table 1 Basic characteristics of the implemented methods

Characteristics	FDM	GFM	PFM	2.5D FEM
Domain	Time	Frequency	Frequency	Frequency
Rail model	Euler–Bernoulli	Euler–Bernoulli	Timoshenko	FEM
Damping model	Viscous	Hysteretic	Hysteretic	Hysteretic
Rail pad length	46 mm	point	180 mm or fuzzy	180 mm or fuzzy

The rail rests on rail pads characterized by stiffness s_p and, depending on the method, either the damping loss factor η_p or the viscous damping coefficient d_p. The masses m_s, representing the sleepers, represent half of the sleeper mass. The spacing between two sleepers is l_s. The effective rail pad length in the X-direction is described by l_c (this does not necessarily correspond to the geometric rail pad length). The ballast is located below the sleepers. It is also described by stiffness s_b and damping properties η_b or d_b. Only vertical bending vibrations of the rail u are considered, except for 2.5D FEM, where also other cross-sectional deformations such as lateral bending and torsion section are considered. All four methods considered in this analysis exclude non-linear effects.

Thompson [1] describes characteristic frequencies for a continuous two-layer model. These characteristic frequencies are also suitable as orientation for the discrete rail model used. The resonance of the rail mass to the pad stiffness is ω_0. The resonant angular frequency ω_1 specifies the resonance of the sleeper mass to the stiffness of the ballast. An anti-resonance occurs at ω_2 and cut-on frequencies at $\omega_{c1/c2}$:

$$\omega_0 = \sqrt{\frac{s_p}{m'_r}}, \qquad \omega_1 = \sqrt{\frac{s_b}{m_s}}, \qquad \omega_2 = \sqrt{\frac{s_p + s_b}{m_s}}, \tag{1}$$

$$\omega_{c1/c2} = \sqrt{\frac{\omega_0^2 + \omega_2^2}{2} \pm \sqrt{\frac{(\omega_0^2 + \omega_2^2)^2}{4} - \omega_0^2\omega_1^2}}. \tag{2}$$

Below ω_{c1} and between ω_2 and ω_{c2}, there is no wave propagation. Another relevant frequency is the so-called pinned-pinned frequency. The wavelength of this frequency corresponds approximately to twice the sleeper spacing l_s [1].

2.1 Finite difference method (FDM)

This finite difference method for bending waves on infinite beams on elastic foundation proposed by Stampka and Sarradj [15] can be used to analyse rail vibrations. The rail is approximated by an infinite Euler–Bernoulli beam (EB). Equation (3) describes the partial differential equation of the bending vibration:

$$\begin{aligned} &EI_r \frac{\partial^4 u(x,t)}{\partial x^4} + m'_r \frac{\partial^2 u(x,t)}{\partial t^2} + d'_r(x)\frac{\partial u(x,t)}{\partial t} \\ &= q(x,t) - s_p(x)(u(x,t) - u_s(x,t)) \\ &\quad - d_p(x)\Big(\frac{\partial u(x,t)}{\partial t} - \frac{\partial u_s(x,t)}{\partial t}\Big). \end{aligned} \tag{3}$$

The transverse deflection u depends on both x, the coordinate along the beam axis, and the time t. E is the rail Young's modulus, I_r is the rail cross-section second moment of area, and m'_r is the beam mass per unit length. q represents the excitation force per unit length, and d'_r is the viscous damping coefficient per unit length of the beam. s_p and d_p are the stiffness and the viscous damping coefficient of the pads. The transverse deflection of the sleeper u_s is given by

$$\begin{aligned} m'_s \frac{\partial^2 u_s(x,t)}{\partial t^2} &= s_p(x)u(x,t) - (s_b(x) + s_p(x))u_s(x,t) \\ &\quad + d_p(x)\frac{\partial u(x,t)}{\partial t} - (d_p(x) + d_b(x))\frac{\partial u_s(x,t)}{\partial t}, \end{aligned} \tag{4}$$

with the mass m'_s of the half-sleepers, the stiffness, s_b and the viscous damping coefficient d_b of the ballast. Note that, for both (3) and (4) stiffness and damping coefficients depend on the coordinate x and thus also non-continuously supported rails can be modelled using appropriate distributions of stiffness and damping along the track.

The system is discretized in space and time, and finite differences approximate the derivatives in the equation of motion. A system of equations is obtained using the implicit Crank–Nicolson method for the time approximation. For a given force excitation, the rail deflection over time can be determined. The detailed method and further information are available in [15].

2.2 Green's function method (GFM)

Nordborg presented the time domain Green's function method [9, 21]. A Green's function is set up for the infinite beam supported on the spring-mass-spring system as described in Fig. 1. Euler–Bernoulli theory is used to model the rail as a beam. The rail is assumed to be periodically supported at discrete points. The system's equation of motion in the frequency domain for free vibration rewritten from [9] for a exp $\mathrm{i}\omega t$ time dependency is:

$$\begin{aligned} &\frac{\partial^4 U(x,\omega)}{\partial x^4} - k^4 U(x,\omega) + \frac{S_{\mathrm{sup}}}{E(1+i\eta_r)I_r} U(x,\omega), \\ &\sum_{n=-\infty}^{\infty} \delta(x - nl_s) = 0, \end{aligned} \tag{5}$$

where $k = \sqrt[4]{\frac{m'_r\omega^2}{E(1+i\eta_r)I_r}}$ is the wavenumber. $U(x)$ is the vertical deflection in the frequency domain and n is an integer. Damping within the rail can be taken into account with the loss factor of the rail η_r.

The dynamic stiffness of the mass-spring-damping-system S_{sup} at the discrete points at frequency ω is

$$S_{\mathrm{sup}} = \frac{S_b - m_s\omega^2}{1 + \frac{S_b - m_s\omega^2}{S_p}}, \tag{6}$$

with $S_p = s_p(1 + i\eta_p)$ and $S_b = s_b(1 + i\eta_b)$. The damping is given by the loss factor η_p of the pads and η_b of the ballast [9].

Equation 5 is adapted to the ballasted track using Floquet's theorem. The result is the Green's function $G_{\omega}(x, x_0)$ of the periodically supported rail. This function can be used to calculate the track's response at point x to an excitation at point x_0. Therefore, this representation in the frequency domain can also be utilized to calculate the track decay rate. The Green's function is transformed into the time domain and then adapted to a moving Green's function in order to analyse the effects of wheel passes [9].

2.3 Point reaction force method (PFM)

Heckl [16] describes a method of supporting an infinite, free Timoshenko beam on a finite number of discrete support systems. Green's functions describe the response of the free beam to a unit point force excitation. The Green's function is formulated in frequency domain [16],

$$G(\mathrm{d}x) = \left(f_{\mathrm{p}}\mathrm{e}^{-\mathrm{i}k_{\mathrm{p}}|\mathrm{d}x|} + f_{\mathrm{d}}\mathrm{e}^{-\mathrm{i}k_{\mathrm{d}}|\mathrm{d}x|}\right)\mathrm{e}^{\mathrm{i}\omega t}, \tag{7}$$

where the first term describes a propagating wave field with wavenumber k_{p} and the second term describes a decaying wave field with wavenumber k_{d}, each with a corresponding wave amplitude (f_{p} and f_{d}, respectively). The method is described in detail by Thompson [1].

Each rail support system is assumed to act on the rail with a point force (Fig. 1). A linear superposition of all forces acting on the free rail, scaled with the corresponding Green's functions, allows evaluating the rail response at any point. Evaluating the rail response at all supports, a linear equation system is obtained, which can be solved for the unknown support forces.

2.4 Waveguide finite element method (2.5D FEM)

The models described above simplify the vibrational behaviour of the rail to that of a bending beam. This reduces the cross-sectional motion of the rail to one or two degrees of freedom, which may be insufficient at high frequencies. A common way to model the cross-sectional behaviour in more detail is the waveguide finite element method [18]. This method lends itself to structures which have a constant geometry along one direction, as the geometry can be represented by a 2D mesh. The finite elements are formulated such that they describe the third dimension of the structure in terms of propagating and decaying waves. In an approach similar to the one by Heckl described above, Zhang et al. [22] coupled a free 2.5D FE-based rail model to a finite number of rail support systems, represented by spring-mass-spring systems.

This article uses an implementation of the discretely supported 2.5D FE-based rail as presented by Theyssen et al. [20]. A total of 119 rail seats are included in the model. Each rail seat is represented by six springs, arranged in two rows. Each row thus consists of three springs distributed over the rail width. Along the rail, each row is located one third of the desired rail pad length from the rail pad centre. The pad stiffness is evenly distributed over all springs The ballast, sleeper and pad stiffness are represented by spring-mass-spring systems using the parameters introduced in the section below.

3 Fuzzy arithmetic

Regardless of how precise a model is working, the accuracy of the input parameters also determines the accuracy of the result. To address the inaccuracy of the input parameters, the general transformation method (GTM), as part of the fuzzy arithmetic, is applied to the models considered. The GTM was introduced by Hanss [10, 23] and has been used for different applications. It is an alternative to other approaches to address uncertainty like the Monte-Carlo method. While the Monte-Carlo method is a powerful method to deal with uncertainty in the sense of randomness, the GTM is more suitable to handle uncertainty in the sense of vagueness.

The Monte-Carlo method, whose accuracy depends crucially on the accuracy of the probability distribution of the input parameters, needs input parameters quantified by probability density functions. However, since these are generally unknown in the present case and can only be roughly assessed at best, this approach is not well suited here and would lead to inaccurate simulation results [11]. Also, for cases similar to the case considered here, the Monte-Carlo method requires a significantly larger number of model evaluations than the GTM in order to achieve the same accuracy of the output results [11]. Therefore, the GTM was chosen here to conduct dynamic track behaviour simulations with several models using fuzzy input parameters. This leads to fuzzy results, which can be understood as the possible range in which the simulation results range for a given parameter uncertainty, but not in the sense of a probability distribution of the results. This range shall be termed here an uncertainty band.

3.1 Fuzzy numbers

The fuzzy arithmetic, based on the theory of fuzzy sets originally introduced by Lotfi Zadeh [24], is the counterpart to conventional arithmetic and uses fuzzy numbers $\tilde{p}$. According to [11], these have the values $\tilde{x}$, to which a functional relationship is assigned. This membership function μ can take values between 0 and 1. However, the membership function does not describe the probability the fuzzy number could take a value but rather defines the spread of these values. Figure 2 shows two examples of fuzzy numbers: a

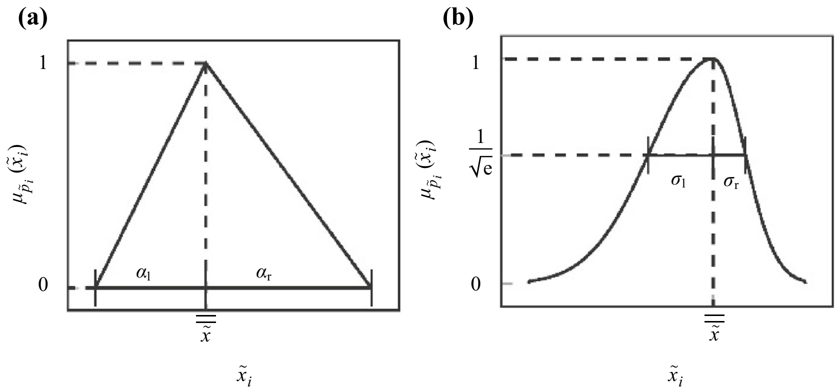

Fig. 2 Two examples for fuzzy numbers: **a** triangular fuzzy number; **b** Gaussian fuzzy number

triangular fuzzy number (tfn) (Fig. 2a) and a quasi-Gaussian fuzzy number (gfn*) (Fig. 2b) with the notation (see [11] pp.47 for more details):

$$\tilde{p} = \mathrm{gfn}^*\left(\bar{\bar{x}};\sigma_\mathrm{l};\sigma_\mathrm{r}\right), \tag{8}$$

where $\bar{\bar{x}}$ describes the peak value of the fuzzy number, which is defined as the value of $\tilde{x}$ where the membership functions become 1. Furthermore, the left-hand and right-hand spread of the membership function is denoted by σ_l and σ_r. The spreads correspond to the standard deviation of the Gaussian distribution.

3.2 General transformation method

In the general transformation method (GTM), the fuzzy parameters are discretized according to a certain procedure [11]. The discrete values of the parameters are used as input parameters for the models. After repeatedly evaluating the model for all those, a fuzzy result, the uncertainty band, is reconstructed from the discrete set of results. Here, the five steps of the GTM are briefly explained. The exact mathematical relationships can be taken from [11].

3.2.1 Decomposition of the input fuzzy number

In the first step, the μ-axis (membership function) is subdivided into $m+1$ levels. As shown in Fig. 3a, this forms the intervals $X_i^{(j)}$ on each level. These intervals form the set, which describes the decomposed fuzzy number. The index i shows the number of considered fuzzy numbers.

3.2.2 Transformation of the input interval

In the second step, the intervals on each μ_j-level are subdivided into discrete points, as shown in Fig. 3b. Thus, each interval $X_i^{(j)}$ of the level μ_j becomes a tuple of discrete values.

3.2.3 Evaluation of the model

The dynamic track behaviour models can now evaluate these discrete values. Considering multiple fuzzy input parameters on each level, all possible combinations of these discrete values are built and considered as tuples with the models. After the simulation, a decomposed and transformed intermediate result is obtained. All intermediate results are summarized in the form of an array.

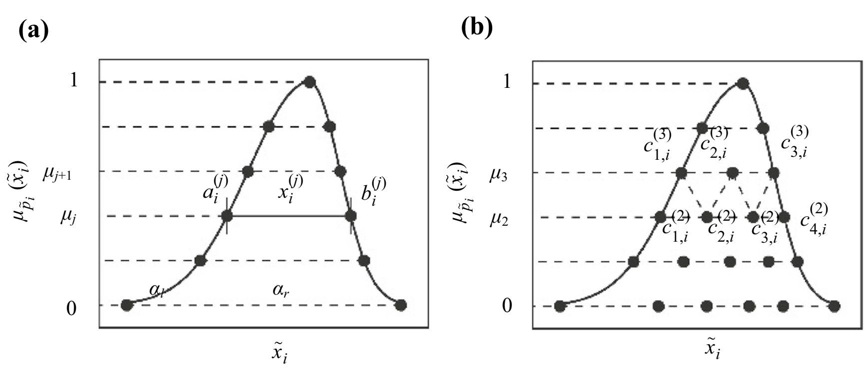

Fig. 3 Examples of steps of the general transformation method: **a** decomposed fuzzy number; **b** decomposed and transformed fuzzy number

3.2.4 Retransformation of the output array

In the next step, the output array resulting from the model evaluation is transformed back. This results in an interval $Z^{(j)}$ per μ_j-level similar to the decomposed fuzzy number $X_i^{(j)}$. The intervals on each μ_j-level form a set of results.

3.2.5 Recomposition of the output intervals

Finally, a fuzzy result in the form of a fuzzy number is reconstructed from the intervals in the set of results. This is done by assigning the single interval $Z^{(j)}$ to the single levels of the membership function μ_j, which finally leads to the fuzzy result.

3.3 Sensitivity analysis

A sensitivity analysis is conducted to quantify the impact of each fuzzy input parameter on the fuzzy result. Therefore, according to [11], additional information contained in the result array is used. Initially, the gain factor $\eta_i^{(j)}$ is determined and converted in the next step into the dimensionless standard mean gain factor κ_i. This quantity is the overall measure of the impact of the single fuzzy input parameters $\tilde{p}_i$ on the fuzzy result. In the last step, the normalized degree of influence ρ_i is determined, depicting each input parameter's relative influence. With ρ_i, it is possible to describe the contribution of each input parameter on the fuzziness of the result. Therefore, each ρ_i ranges between 0 and 1 and the sum of all ρ_i has to be equal 1 ($\sum_{i=1}^{n} \rho_i = 1$).

4 Fuzzy parameter application to simulations of a ballasted track

Hereafter, the parameters required to simulate bending vibrations in the vertical direction are presented, based on the models described in Sect.2. It is analysed how precisely these parameters can be specified for predicting the point input mobility mid-span and the TDR with the hammer impact method [2] and whether these parameters are to be regarded as fuzzy. A summary is shown in Table 2.

The GTM is not well suited to deal with the uncertainty that is introduced by the variation of parameters along the track. Therefore, the present analysis does not take this into account. Interested readers are referred to the literature [25], where the effect of parameter variation along the track on both mobility and track decay rate is discussed in detail.

4.1 Rail parameters

The Euler–Bernoulli model for the rail is characterized by the mass per unit length m'_r, which can be determined from the density of the rail ρ and the cross-sectional area A_r, Young's modulus E, and the internal damping (d'_r or η_r, see Appendix A), and the second moment of area I_r. The Timoshenko beam model additionally requires the shear modulus G. The 2.5D FE model is defined by its geometry and material properties, including the density ρ, E, ν and material damping η_r.

The parameters ρ, E, ν, and G of the rail are material-dependent parameters [26, 27]. Since the steel grades used for the profiles are predefined [28], a significant variation of these parameters is not to be expected. This analysis does not consider these parameters' temperature dependence. However, this might be relevant in specific scenarios.

Regular grinding of rails is necessary to prevent rail defects. Material is removed from the rail head by grinding and wear caused by passing wheels over the rail. This, in turn, reduces the rail's mass and second moment of area during its use [5]. Depending on the track category and train speed, the operator guideline [29] specifies wear of the track in the vertical direction of 10–20 mm, which requires maintenance and repair work of the rail. Therefore, the cross-sectional area A_r and the second moment of area I_r and thus, the mass m'_r can be assumed to be fuzzy parameters. However, if the profile has been measured, these parameters can be assumed to be fixed.

Damping affects the wave propagation in the rail. It can be specified by the loss factor η_r or the viscous damping coefficient d'_r. The two quantities can be approximately converted into each other at specific frequencies; see more details in A. In the literature, the loss factor for steel is typically reported as very low, ranging from 0.2×10^{-4} to 3×10^{-4} [30–32]. However, comparing measurement data with simulations has shown that this value is too small for most modelling approaches [7]. This could be because additional energy losses occur; for example, when fastening the rail foot with the fastener, it must be added to the loss factor [7]. Coherence with measurements seems to be achievable with a loss factor of the rail in the range of 0.01–0.03 [7, 31, 33]. Since the loss factor of the rail is only roughly estimated, this parameter can be classified as a fuzzy parameter.

4.2 Rail pads parameter

The properties of the pads are described by their dynamic stiffness, damping, and effective rail pad length.

4.2.1 Pad stiffness

Generally, the dynamic stiffness of pads can vary over a wide range from very soft at $60\,\mathrm{MN}\cdot\mathrm{m}^{-1}$ [34] to very stiff at $3500\,\mathrm{MN}\cdot\mathrm{m}^{-1}$ [35], the latter implying that the pads are almost as stiff as if no pads were used at all [36]. However, individual pads do not vary over this wide range.

The stiffness depends slightly to moderate on the preload, in dependence on the material and geometries of the pads [34, 37–39]. The load results from the toe load with the help of the clips and from the train's weight during a pass. The preload induced by the clips is the only decisive factor in the investigations considered in this work, where the TDR is analysed using the hammer impact method. The preload decreases over time, caused by the loosening of the clips [40] and reducing the pads' stiffness. Furthermore, a deviation up to ± 12% of the nominal preload can be caused by the malposition of the clips [41].

Moreover, the stiffness of the pads decreases due to ageing effects. Thus, Kaewunruen and Remennikov [39] found a decrease of about 4% per year for the frequency-independent static stiffness; no clear correlation could be identified for the measured frequency-dependent stiffness. According to [42], a comparison of new and 10-year-old pads showed a significant decrease in stiffness. This effect is further increased by a thinning of the pads over time due to load changes, which in turn causes a significant reduction in toe load, and thus, the effective rigidity further decreases [42].

The track can show a temperature difference of well over 20 °C throughout a day [4]. Depending on the pad's material, the stiffness of the pads can vary significantly with the temperature [37]. A temperature increase can decrease the stiffness up to 13%, and an increase of up to 24% of the stiffness is described when the temperature is reduced [37].

The stiffness of the pads is also significantly dependent on the frequency and amplitude of the rail vibration [34]. The stiffness increases strongly with frequency [37, 43]. Frequency domain simulations would allow the stiffness to be specified as a function of frequency. This implies that the frequency dependence would not lead to any fuzziness in the stiffness. However, if the stiffness is reduced to a single number value, as required for time domain models, it is unclear how this should be estimated from the frequency-dependent stiffness. Therefore, a single number value results in uncertainty.

Since only relatively small amplitudes of rail deflection are expected using the hammer impact method for measuring the TDR, the influence of the rail deflection amplitude on the stiffness is assumed to be so small that a negligible effect can be expected.

However, a significant problem is that even a known pad is found to have different values with different measurement methods [43, 44]. On the one hand, the pad stiffness can be determined statically or dynamically in a test rig [43]. On the other hand, the stiffness can also be determined in field measurements. A third option is to use a curve-fitting procedure to adjust the stiffness, as well as other parameters, such as the damping, in a model to ensure that a parameter curve, e.g. of the point input mobility, fits the measured values well [7]. The reason for the differences between the various measurements could also be that the standard deviation of the pad stiffness for different pads of the same type, according to Oscarsson [45] and Fenander [43], is relatively high at about 14%.

A comparison of field and laboratory measurements shows that the field measurements yield values almost two

Table 2 Assessment of the rail and superstructure parameters on the level of uncertainty

Parameters	Level of uncertainty	Causes of uncertainties
Rail density ρ	Low	Temperature
Rail cross-sectional area A_r	Low to significant	Grinding and wear
Rail shear modulus G	Low	Temperature
Rail static Young's modulus E	Low	Temperature
Rail internal damping d_r' or η_r	Significant	Additional energy loss
Rail second moment of area I_r	Low to significant	Grinding and wear
Pad stiffness s_p	High	Temperature, frequency, age, preload, measurement method, and/or installation situation
Pad damping d_p or η_p	Significant	Temperature, frequency, age, preload, measurement method, and/or installation situation
Rail pad length l_c	Significant	Effective length unknown
Ballast stiffness s_b	High	Frequency, age, preload, measurement method
Ballast damping d_p or η_p	Significant	Installation situation, (frequency), and/or preload
Sleeper mass m_s	Low	–

times larger than the laboratory measurements [43]. Furthermore, it is also shown that if the stiffness is estimated from the point input mobility of measurements, it is significantly higher than the stiffness determined by direct measurement methods [1]. Depending on the chosen measurement method, the stiffness values can thus vary by up to 50% [44]. Therefore, assuming an average value of the pad stiffness is challenging even for a specific pad. Hence, the pad stiffness must be classified as a highly uncertain parameter with a wide variance. Selecting the variance depending on the method of determining the stiffness seems advisable here. Assuming the pad type or stiffness is only known from laboratory measurements or different installation situations, the mean stiffness value already varies considerably because the stiffness in the installation situation can only be roughly estimated. Additionally, variances may result from the parameters age, temperature, preload, and due to the uncertainty when reducing the stiffness to a frequency-independent value. Therefore, a variance of ± 50% of the mean value seems adequate in the fuzzy prediction.

A significantly lower variance can be specified for rail pad stiffness determined with a curve-fitting method from measurement data from the track. This method defines the stiffness in the specific track situation. However, there are also uncertainties in this method. On the one hand, the pad stiffness varies along the track. For example, if the clip is unfastened at the measuring position, the resulting pad stiffness may not represent the entire track. On the other hand, the curve-fitting procedure provides an approximation because various parameter combinations can result in similar results in the curve of, e.g. point input mobility. An estimation is problematic if the frequency ω_{c2}, to which the stiffness is usually fitted, coincides with the pinned–pinned frequency. A variance range of ± 25% to the determined value seems appropriate for the pad stiffness estimated by the curve-fitting method. However, other factors, such as temperature, must also be considered.

4.2.2 Pad damping

The damping of the pad has no direct relation to the stiffness of the pad [6, 44]. For different pads, the damping coefficient is given between 5 kNs/m^{-1} and 70 kNs/m^{-1} [6] or as loss factors between 0.1 up and 0.6 [6, 44]. For the damping of the pads, similar to the stiffness, it was determined that the measured loss factors also depend on the measurement method. For example, Thompson and Verheij [35] concluded that when the loss factors are determined from field measurements, the values are twice as high as values for measurements in a test rig. In [1], values of the loss factor of 0.2–0.25 are given, determined via a curve-fitting method of the point input mobility. In measurements of the individual pads, the values were significantly lower at 0.1–0.15 [35, 38]. Also, in [44], it is shown that the loss factors determined by curve-fitting methods from field measurements are significantly higher with 0.25–0.3. However, the variance in measurements utilizing equal pads is significantly lower than for the stiffness [43].

The relationship between loss factor and frequency does not seem to be straightforward. In [39], it is stated that the damping coefficient decreases with frequency. Thompson et al. [44] describe that no direct correlation between frequency and damping can be found. However, Fernander [43] discusses a soft pad for which the loss factor of up to about 300 Hz hardly depends on the frequency. Above 300 Hz, the loss factor increases significantly as a function of the preload [43]. Another measurement of the same pad, for instance, does not indicate an influence of the preload on the loss factor [43]. An independence of damping from preload is also observed in [44].

Depending on the material, the loss factor also correlates with the temperature. For example, Squicciarini et al. [4] found that the loss factor could be increased from 0.15 at 40 °C to 0.6 at − 20 °C. The damping coefficient is reported in [39] to decrease by 0.09 kNs/m per year of operation (with an initial value of 4.1 kNs/m), which corresponds to a decrease of about 2% per year.

Therefore, the specification of a mean value for rail pad damping also has high uncertainty. However, the variance due to other influences such as age and preload seems less than for the stiffness. Depending on the material, the temperature has a significant influence, leading to uncertainties. Specifying a single damping value can also lead to uncertainty depending on the material. For the loss factor, a range of 0.1–0.3 seems reasonable, independent of the pad, since the pads have only been recorded with these values for various measurement methods in the literature, apart from a few exceptions for which higher values were given [6, 35, 43, 44]. This variance must be increased if very low temperatures are not excluded.

4.2.3 Effective length of the rail pad

The geometric length of the pad can be specified if the pad type is known. However, the effective length of the pad l_c, i.e. the length over which a constant pad stiffness can be assumed, is unknown. This is primarily because the pads protrude beyond the dimensions of the sleeper. The effective length of the rail pad in the X-direction l_c should be considered (if allowed by the model) to get a more precise calculation of the pinned–pinned frequency [46]. Depending on the rail pad type, the length varies in the outer dimension between 134 and 230 mm according to the manufacturer [47], with the inner dimensions being 10–15 mm smaller. The minimum effective length is considered the inner dimension of the rail pad because, in this area, both the rail and the sleeper are in complete contact with the pad. The maximum effective length can be equated with the outer dimension, even if it needs to be expected that the edge area of the pad no longer has the specified stiffness. A specific nominal value cannot be given, as no research on the influence of this edge area could be found. Therefore, the effective rail pad length in X-direction l_c can also be considered a fuzzy parameter.

4.3 Ballast parameters

The ballast is modelled as a linear spring described by its stiffness and damping. The measurement of these parameters is more complex than for the pads and is therefore often determined with curve-fitting methods from measured data [8, 44, 48]. Zhai et al. [49] presented a calculation method for the ballast stiffness. However, specific values are necessary to calculate the stiffness, such as the ballast depth or the half sleeper's effective supporting length. Often, these ballast values are unknown. Therefore, this calculation method can only be used in rare instances.

Generally, the ballast stiffness varies over a range of 12–500 $\mathrm{MN \cdot m^{-1}}$ [6, 22, 45]. However, values between 30 and 150 $\mathrm{MN \cdot m^{-1}}$ are most frequent [6, 35, 44, 48, 50]. For laboratory measurements, the range of stiffness is significantly larger (12–500 $\mathrm{MN \cdot m^{-1}}$) than for values calculated from passing measurements (35 to 65 $\mathrm{MN \cdot m^{-1}}$) [6]. However, there seems to be significantly less deviation between direct and indirect measurement methods for ballast stiffness than for pad stiffness [22]. The values for the ballast stiffness are also strongly frequency-dependent [34]. Therefore, the same problem occurs if only a single value is specified, such as for the pad stiffness.

Increasing the preload results in a partly significant increase in stiffness [22]. For a 1.86 kN preload on the ballast by the mass of the sleepers, Wu and Thompson [34] determined the stiffness with 15 $\mathrm{MN \cdot m^{-1}}$ to 80 $\mathrm{MN \cdot m^{-1}}$ depending on frequency. The stiffness also varies over time. For example, in [35], a measurement was repeated after 10 months, showing a reduction by a factor of three. One reason may be the contamination of the ballast by clay sub-grades, which reduces the stiffness [51]. Other factors, such as stone blowing, can result in a modification of the ballast over time so that the ballast stiffness can vary between 7 and 15 MPa [52].

Because of the strong frequency dependence, Thompson [1] considers the viscous damping model as advantageous for describing the damping effect of the ballast. In [22], however, it is stated that the ballast damping is primarily independent of the frequency. The damping of the ballast also seems to vary considerably. A loss factor from 0.2 to 2.0 [6, 36, 44] or a viscous damping coefficient from 30–240 kNs/m [6] can be found in the literature. Most of the values were determined by curve-fitting methods [8, 44, 48]. However, there is no direct dependence between the measurement method and the obtained damping values [22]. The damping of the ballast is slightly increased by the preload [22].

The stiffness and damping of the ballast are, consequently, hard to specify. The interval needs to be set at a wide range if no precise information can be obtained about the ballast. For values determined by curve-fitting, with the same restrictions as for the stiffness of the pads, it can be assumed that this value corresponds to the specific setting. An uncertainty of up to ± 40% must be assumed when determining the ballast stiffness using the curve-fitting method. A range of 0.2–2 can be assumed for the loss factor if curve-fitting does not estimate the damping. An uncertainty of ± 50% seems appropriate even for values that could be estimated from measured data.

4.4 Railway sleeper parameters

For the four models considered here, the mass and distance are the most critical parameters of the sleeper. DIN EN 13230-1 [53] prescribes a maximum deviation from the given mass of ± 5%.

Often, half the mass of the complete sleeper is given as the operating mass for the spring-mass-spring system. However, the operating mass may deviate from this. Due to, e.g. an uneven distribution of the mass on the ballast, the operating mass for one side can be larger or smaller than half the sleeper mass. According to [54], the pressure in the contact between the monoblock sleeper and ballast is not distributed symmetrically between the two rails. Therefore, the mass is also not divided equally under both rails. This phenomenon varies from sleeper to sleeper along the track and should not be relevant on average. According to [55], concrete sleepers are so durable that no significant mass decrease is expected due to corrosion. Thus, a deviation of ± 5% is expected so that the sleeper mass can be treated as a non-fuzzy parameter.

Deviations of the sleeper spacing along the rail are documented in [1]. However, these deviations are more stochastic and not systematic. Therefore, the sleeper spacing is not to be evaluated as fuzzy.

5 Implementation of the GTM for the determination of the TDR on a ballasted track

A dataset of measurements on a ballasted track and accompanying track parameters by Li et al. [7, 56] was used as a reference to demonstrate the application of the fuzzy parameter approach. The measuring of the point mobility mid-span and the TDR with the hammer impact method were part of the measurements of Li et al. [7, 56]. The TDR measuring procedure using the hammer impact method is described in [2].

5.1 Measurement data of a ballasted track

The measurements by Li et al. [7] were realized in May 2015 in the UK on a UIC 60 rail with bi-block sleepers, whose mass per sleeper end is 120 kg. No specific information is available on either the ballast or the pads. The distance between the sleepers is given as 0.6 m. To approximate the parameters of the pad and ballast, the point input mobility was determined and compared with a wavenumber finite element simulation (very similar to the 2.5D FEM used here). The parameters pad stiffness, pad loss factor, ballast stiffness, ballast loss factor, and the loss factor of the rail were thus approximated [7]. The values given in [7] are assumed to be mean values for the fuzzy parameters.

5.2 Determination of the fuzzy numbers

In the following paragraphs, the fuzzy values for the required parameters are determined.

The age and condition of the rail are not specified, so the wear cannot be estimated. Therefore, a wide variance range is defined. The rail cross-sectional area A_r, or rather the rail mass m'_r and the second moment of area I_r depend essentially on the height of the rail profile h_r. For the FDM, GFM and PFM, the relationship between the rail mass and the profile height are assumed to be approximately linear. The second moment of area is roughly described as proportional to h_r^3. The nominal values of the rail are given for the rail type UIC 60 for a new rail and a worn rail in Table 3. Based on these values, the following correlations were determined:

$$I_\mathrm{r} = \frac{0.071644\,\mathrm{m}}{12} h_\mathrm{r}^3 \tag{9}$$

$$m'_\mathrm{r} = \frac{6.31\,\mathrm{kgm^{-1}}}{0.0094\,\mathrm{m}} h_\mathrm{r} - 55.249\,\mathrm{kgm^{-1}} \quad . \tag{10}$$

$$A_\mathrm{r} = \frac{0.0008\,\mathrm{m}^2}{0.0094\,\mathrm{m}} h_\mathrm{r} - 0.006968\,\mathrm{m}^2. \tag{11}$$

In [29], a maximum wear of 14 mm is given for UIC 60 rails for an intermediate speed range of the train from 80 to 120 km/h. Measures must be taken on the track above this reduction in profile height. Therefore, a profile height reduction of 14 mm is assumed as the minimum. The maximum mass and second moment of area of the rails are determined by the nominal dimensions [28]. A moderate mean abrasion of 5 mm is assumed. The resulting rail masses and second moment of area values are provided in Table 4.

Note that for models calculated with the EB-beam assumption (GFM and FDM), the second moment of area is reduced by 40%. This is a simple procedure to compensate for the deviations caused by the EB-beam model at higher frequencies [9]. In the 2.5D FE model, wear is approximated by altering the geometry of the rail head. As an example, two meshes of the rail are shown in Fig. 4.

The rail loss factor in the installation situation is specified as 0.01 in [7]. The rail loss factor could be significantly lower, so the minimum is set to 0.001. The maximum is set to 0.03, corresponding to the highest value in the literature [33]. The viscous damping coefficient for the rail is calculated from the rail loss factor and the rail mass, assuming a pinned-pinned frequency of 1100 Hz (see appendix A, Table 5).

The dynamic stiffness of the pads is given as 600 MN $\mathrm{m^{-1}}$ in [7], corresponding to a moderate stiffness. Due to the curve-fitting method, an approximate deviation of ± 25% can be assumed. The damping of the pads was estimated with a loss factor of 0.25 [7]. As explained in Sect. 4.2, a variance range of 0.1–0.3 is applied. Since the measurements took place in May in the UK, very low temperatures are not expected and a larger estimation range is not required. The respective viscous damping coefficient is determined from the loss factor and the rail pad stiffness according to Table 5.

The pad length was not specified in [7]. For UIC 60 rails, pads have an outer dimension of 134–230 mm, most commonly 180 mm. Therefore, these values are used as the variance range and the mean value. This broad estimate would not be considered necessary if the pad type or the rail pad dimensions were known. For the calculations with GFM, only a point support can be considered; see Chapter 2.2. The rail pad length for the FDM can only be multiples of the

Table 3 Parameters of an UIC60 rail

Parameters		New rail E1 [28]	New rail E2 [28]	Worn rail E1 [57]
Mass per m length (kg/m)	m_r	60.21	60.03	53.9
2nd moment of area (m^4)	I_r	30.381×10^{-6}	30.2151×10^{-6}	25.261
Rail height (mm)	h_r	172	172	162.6
Cross-sectional area (cm^2)	A_r	76.7	76.48	68.7

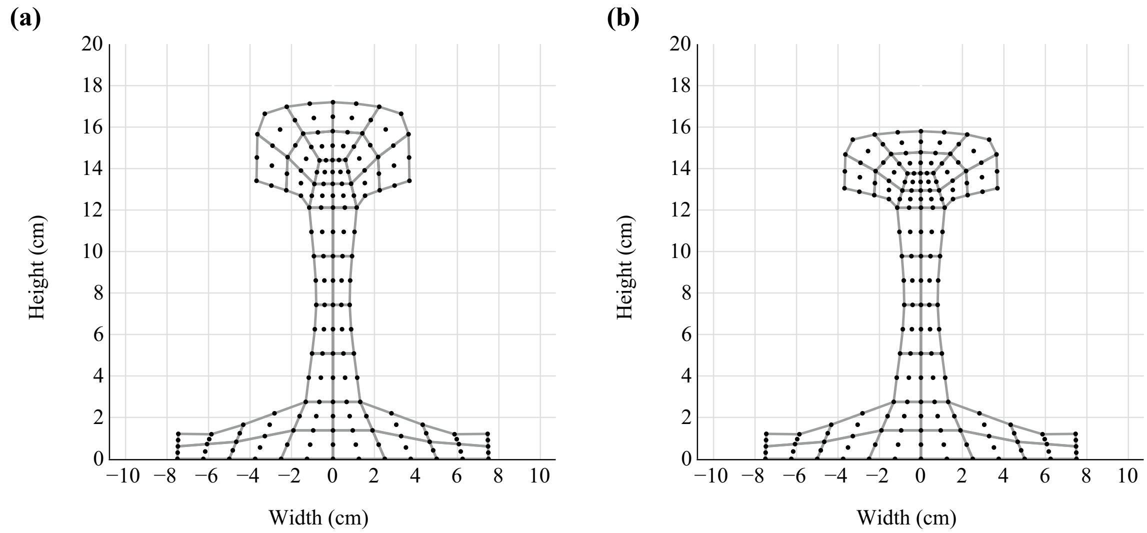

Fig. 4 Discretisation of the cross-section in the 2.5D FEM approach: **a** full UIC60 172 mm height; **b** worn UIC60 158 mm height

Table 4 Clear and fuzzy track parameters (unloaded)

Track parameter	Symbol	$\bar{\tilde{x}}$	σ_l	σ_r	Unit
Rail Young's modulus	E	210	–	–	GPa
Rail shear modulus	G	80.8	–	–	GPa
Rail density	ρ	7850	–	–	$kg \cdot m^{-3}$
Rail profile height	h_r	167	158	172	mm
↪ Mass per m length	m'_r	(56.9)	(50.81)	(60.21)	$kg \cdot m^{-1}$
↪ 2nd moment of area	I_r	(27.81)	(23.54)	(30.38)	Mm^4
↪ 2nd moment of area (EB-beam)	$I_{r,\,EB}$	(16.69)	(14.12)	(18.23)	Mm^4
↪ Cross-sectional area	A_r	(7.24)	(6.48)	(7.67)	$10^{-3}\ m^2$
Rail loss factor	η_r	0.01 [7]	0.001	0.03	1
↪ Viscous damping coefficient*	d'_r	(3.9)	(0.39)	(11.8)	$kNs \cdot m^{-2}$
Rail shear correction coefficient	κ	0.4	-	-	1
Rail pad stiffness	s_p	600 [7]	450	750	$MN \cdot m^{-1}$
Rail pad loss factor	η_p	0.25 [7]	0.1	0.3	1
↪ Viscous damping coefficient*	d_p	(35.8)	(14.3)	(42.9)	$kNs \cdot m^{-1}$
Rail pad length (2.5D FE and PFM)	l_c	180	134	230	mm
Half sleeper mass per rail	m_s	120 [7]	-	-	kg
Fastener spacing	l_s	0.6 [7]	-	-	m
Ballast stiffness per fastener	s_b	42 [7]	25.5	58.8	$MN \cdot m^{-1}$
Ballast loss factor	η_b	1.0 [7]	0.5	1.4	1
↪ viscous damping coefficient*	d_b	(71)	(35.5)	(99.4)	$kNs \cdot m^{-1}$

Parameters in bold are fuzzy. Parameters with an arrow in front are derived from those of the parameters above and σ values are only illustrative; viscous damping parameters marked with a * are derived from multiple other parameters (see Appendix A) and $\bar{\tilde{x}}$ values are given for peak values of these parameters only; rail profile parameters are not used for the 2.5D FEM

spatial increment d_x and is fixed to one $d_x = 0.046$ m. The fuzziness of the rail pad length in the x-direction is considered for the PFM and 2.5D FEM. In the PFM, each rail pad is represented by two springs in the longitudinal direction of the rail with a spacing of two-thirds of the intended rail pad length. In the 2.5D FEM, the same longitudinal spacing is used for two rows of each three springs distributed across the rail foot. The 2.5D FE model requires an additional lateral constraint. This is achieved by introducing a lateral pad

Table 5 Conversion of loss factors to viscous damping coefficient

Component	Relevant frequency	Viscous damping coefficient d
Rail pad η_{p}	ω_0	$d_{\mathrm{p}} = \frac{\eta_{\mathrm{p}} s_{\mathrm{p}}}{\omega_0} = \eta_{\mathrm{p}} \sqrt{s_{\mathrm{p}} m_{\mathrm{r}}}$
Ballast η_{b}	ω_1	$d_b = \frac{\eta_{\mathrm{b}} s_{\mathrm{b}}}{\omega_1} = \eta_{\mathrm{b}} \sqrt{s_{\mathrm{b}} m_{\mathrm{s}}}$
Rail η_{r}	$\omega_{\mathrm{c2}}; \omega_{\mathrm{p-p}}$	$d'_{\mathrm{r}} = \eta_{\mathrm{p}} m'_{\mathrm{r}} \omega_{\mathrm{p-p}}$

and ballast stiffness equivalent to a tenth of the vertical stiffnesses, to which the nodes on the rail foot are coupled.

The mass of the sleeper and the distances between the sleepers are assumed to be specific parameters obtained from [7].

The stiffness of the ballast is given as $42\,\mathrm{MN} \cdot \mathrm{m}^{-1}$. As described in Sect. 4.3, a deviation of approximately $\pm$ 40% is assumed. Since an exact damping specification is demanding, this parameter is specified by a wide variance with a loss factor of 0.5–1.4. The corresponding damping coefficient is calculated using Table 5.

All parameters are estimated as quasi-Gaussian fuzzy numbers, due to the lack of specific information. All parameters and fuzzy values are summarized in Table 4.

6 Results

For all four models, the point input mobility and the TDR according to EN 15461 [2] were calculated. Parameters describing the track can be found in Table 4. The numerical specifications are presented in Appendix B. Three μ_j levels were determined to minimize the computational effort in calculating the fuzzy results.

6.1 Fuzzy results and sensitivity analysis with all fuzzy numbers simulated with PFM

All parameters identified as fuzzy were included in the PFM simulation. Considering only the peak values ($\mu_j = 1$), i.e. the curve that would result if only the fixed parameters were included in the simulation, an obvious deviation can be observed between the simulation results and the measured curve for the point input mobility, see Fig. 5a. In particular, the peak of the frequency ω_{c2} is shifted from 640 Hz for the measurements to a higher frequency of 740 Hz in the simulation, indicating that the stiffness of the pads has been overestimated. The uncertainty band of the fuzzy result is relatively large over the whole frequency range (see Fig. 5a). There is no frequency range that is not affected by this consideration. In general, the fuzzy simulation results can reproduce the measured curve well. However, despite the assumed high dispersion of the input parameters, the measured curve cannot be explained in all frequency ranges. On the one hand, the model may not capture all the influencing factors that affect the point input mobility in these frequency ranges thus leading to mismatches. On the other hand, the curve-fitting procedure was implemented with a different model. Therefore, the input parameters of the model used may are not sufficiently fitted. As some of the initial values were taken from [7] and not precisely adjusted, and only one measurement curve can be used for comparison in each case, it is impossible to provide any information about the quality of the method in this study. By using the measured data in comparison with the simulated data, only an impression of the applicability of the GTM can be given.

The $\mu_j = 1.0$ curve of the TDR also differs significantly from the measurement (see Fig. 5b). However, the uncertainty band of the result can justify the measurement curve for a wide frequency range. In the medium frequency range between 300 and 700 Hz, the model tends to overestimate the measured curve and thus predicts a significantly stronger decay of the vibrations along the rail (see Fig. 5b). This might be caused by the assumption of equidistant superstructure properties for all sleepers, leading to a pronounced blocked band. In the real superstructure, it can be assumed that, for example, the stiffness varies along the track and thus leads to a weakening of the blocked band. This variation along the track is not included in the fuzzy results.

The sensitivity analysis (see Fig. 5c and d) shows that rail wear (captured by the profile height h_{r}) is the most influential parameter on the result over a large frequency range. As expected, based on the literature, the stiffness of the rail pads strongly influences the result, while the stiffness of the ballast only influences the result in the lower frequency range.

The frequencies at which the measurement curve cannot be explained by the fuzzy results differ between the point input mobility and the TDR, see Fig. 5a and b. Therefore, conclusions cannot be drawn from one variable to the other. A stronger correlation between the point input mobility and the TDR was expected, as the TDR is determined from the ratio of point input mobility to transfer mobilities. On the one hand, the measured point mobility may not be representative of the track. On the other hand, it can be assumed that the transfer mobilities are influenced by different parameters than the point input mobility. Comparison of the Fig. 5c and d also indicates this correlation. The influence of the uncertainty of the various parameters on the total result differs between the point input mobility and the TDR. For example, the impact of the damping values is more significant for the calculation of the TDR than for the point input mobility in a broader frequency range. Thus, the uncertainty of η_{r} has almost no influence on the result for determining the point input mobility. Nevertheless, the fuzziness of

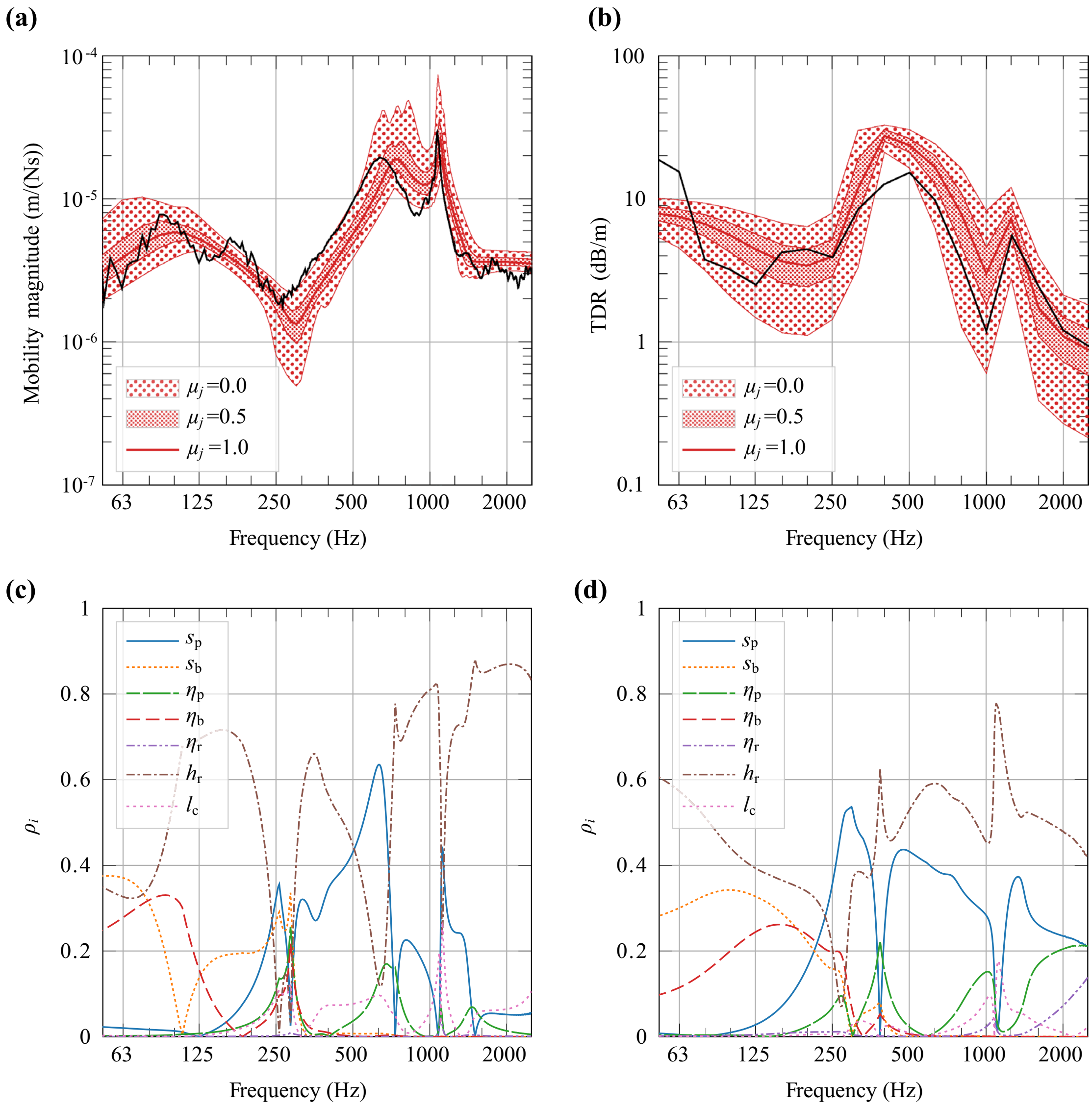

Fig. 5 Fuzzy results and sensitivity analysis of point input mobility and TDR for the fuzzy numbers of s_p, η_p, s_b, η_b, η_r, h_r , and l_c simulated with PFM; black lines indicate the measured data [7]: **a** point input mobility mid-span; **b** TDR; **c** degree of influence point input mobility; **d** degree of influence TDR

the rail damping influences the results above the pinned-pinned frequency when calculating the TDR. However, the other parameters influence the results for the point input mobility or the TDR with varying degrees of sensitivity depending on the frequency.

6.2 Comparison of all four simulation methods with fuzzy numbers

The parameters s_p, η_p or d_p, s_b, η_b or d_b, η_r and h_r have been considered as fuzzy numbers for all four simulation methods. It should be noted that the effective rail pad lengths of the track are different in the various models (see Sect. 5.2).

The simulation results for the point input mobility for the four methods are shown in Fig. 6. In the results based on the peak values for the input parameters, where $\mu_j = 1.0$, only the 2.5D FEM provides a close agreement over the entire frequency range between the simulated point input mobility and the measured curve. This is primarily caused by the fact that the curve-fitting procedure in [7] uses a very similar method. However, this good agreement also requires that the spring elements that model the pad are distributed in the same way as it was done in [7]. For all other methods, which use only one spring over the rail width, the resonant frequency ω_{c2} is overestimated.

The direct comparison, Fig. 7 shows that the 2.5D FEM and the PFM can estimate the measured curve over a wide

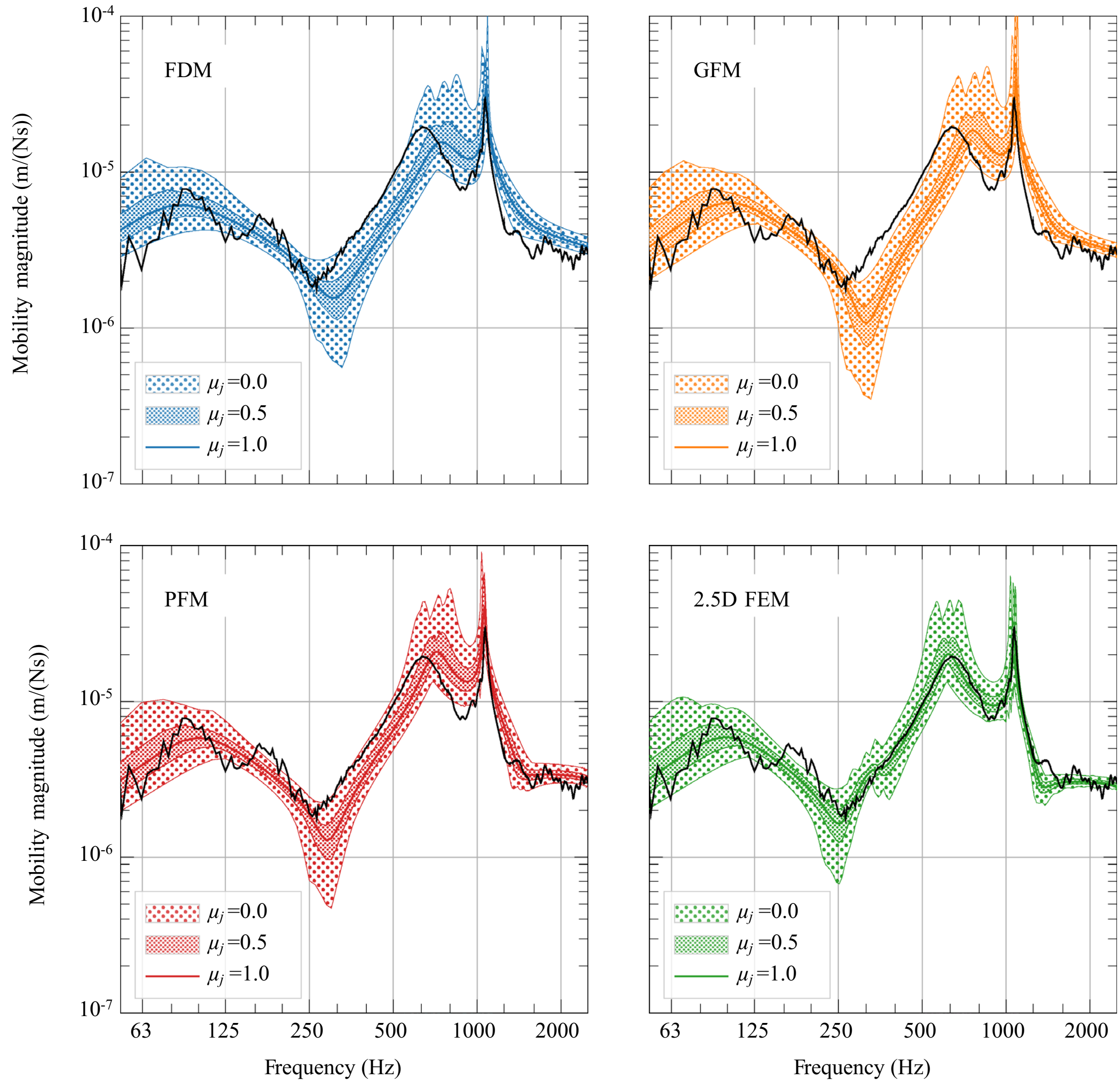

Fig. 6 Fuzzy results of point mobility mid-span for the fuzzy numbers of s_p, η_p, s_b, η_b, η_r , and h_r for all four models; black line indicates the measured data

frequency range if the fuzzy results are considered and the 2.5D FEM shows the best agreement in the medium frequency range from about 200 to 1250 Hz.

The two methods based on the EB-beam (FDM and GFM) show similar trends regarding the deviation from the measured results, see Fig. 7b. The differences between them might be attributed primarily to the different damping models. Especially in the frequency range above the pinned–pinned frequency, the two EB-beam models (FDM and GFM) demonstrate significantly more deviations from the measurement curve than the Timoshenko beam model (PFM). This is because the bending vibrations calculated with the EB-beam model deviate significantly from the actual vibration behaviour at high frequencies [1].

Furthermore, the results indicate that there are frequency ranges in which no method can explain the measurement curve despite considering the fuzzy parameters, such as in the range between ca. 100 and 200 Hz and no model explains the measurements over the full frequency range. So, some mechanisms cannot be detected by any method with the chosen parameter values, or the differences between simulations and measurements are due to possible measurement errors.

As can be seen in Fig. 8, none of the simulations' peak value curves $\mu_|j| = 1$ match the measured TDR very well, even if the curves are similar. As observed for the PFM, all methods overestimate the blocked band between 300 and 800 Hz. Again, the FDM and GFM results are quite similar, as both methods are based on the EB-beam model. The GFM provides significantly smaller TDR values below 200 Hz than the FDM. A possible reason for this could be the influence of the different damping models. The maximum of the

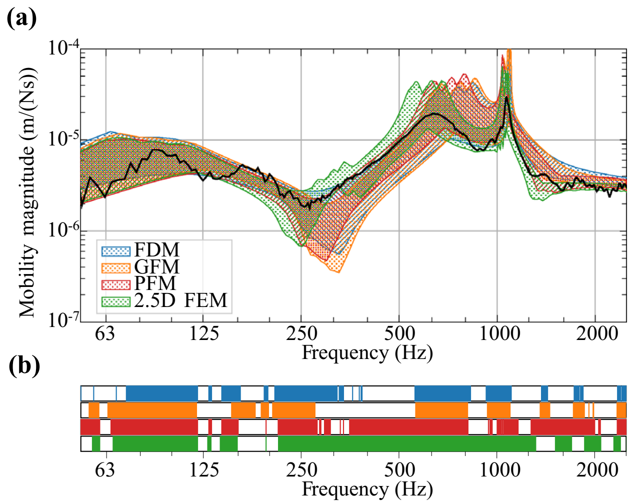

Fig. 7 Comparison of uncertainty bands of results of point mobility mid-span for the fuzzy numbers of s_p, η_p, s_b, η_b, η_r , and h_r: **a** black line indicates the measured data; **b** error of the fuzzy result, white areas indicate that the fuzzy results cannot explain the measurement curve

PFM and 2.5D FEM TDR values are shifted to lower frequencies than the measurement curve.

However, considering the fuzzy result, the measured curve agrees with the measurement results for a wide range of frequencies for all four methods. Comparing Figs. 7 and 9, it is noteworthy that the fuzzy results of the FDM with the used parameters can explain the measurement curve of the TDR at most frequencies, and the 2.5D FEM shows less agreement. However, this is contrary to the results of the point input mobility. This also demonstrates that it is not meaningful to make a statement about the quality of the models based on the data used here. The various methods indicate differences regarding the influence of the fuzzy parameters on the fuzzy result over the frequency (see Figs. 10 and 11), even if the curves can be judged as generally similar.

In the frequency range around 2.5 kHz all four methods show similar trends: The uncertainty bands for the point mobility are narrow, and the sensitivity to all track parameters except the rail profile height is small. The uncertainty bands for the track decay rate become relatively wide, and the most important influence on uncertainty is the rail profile height. It can be concluded that for higher frequencies the properties of the rail itself are important for the results and thus are also responsible for their uncertainty. However, for the sake of clarity the present study does not provide results above 2.5 kHz. For both the GFM and the FDM the EB-beam assumptions are no longer valid in that frequency range and results become less meaningful. While the PFM and 2.5D FEM assumptions are still valid, additional details of the cross-sectional geometry of the rail not reflected in a simple change of rail height will have some influence on the result and would need to be considered in the analysis as additional fuzzy parameters.

6.3 Influence of the effective rail pad length as a fuzzy parameter with 2.5D FEM

The influence of the effective rail pad length l_c as a fuzzy parameter was analysed in more detail under the assumption that the wear is known and therefore not included as a fuzzy parameter, see Fig. 12.

The effective rail pad length l_c is a non-negligible parameter in the pinned–pinned frequency range for both simulations of the TDR and the point input mobility, as shown in Fig. 12c and d. Increasing the effective rail pad length increases the pinned-pinned frequency with a lower amplitude of the point input mobility. An influence of the rail pad length l_c is already observed for frequencies above 300 Hz.

7 Discussion

The common practice of assuming fixed values for the input parameters for the calculation of the rail vibrations only yields satisfactory results for the calculation of the point input mobility with the 2.5D FEM, which was in turn used as the basis for determining the fixed values, see Fig. 6. However, determining the TDR with the 2.5D FEM gives not completely satisfactory results, Fig. 8. The calculation of the point input mobility or the TDR using the fixed input parameters cannot provide satisfactory results for any of the other methods, see Figs. 6 and 8. Even though it would be possible to determine the parameters for the other methods using curve-fitting, this would not be possible for a prediction, for example, and it would be necessary to base the prediction on existing values.

Since the input parameters uncertainty is considered, the measurement results in wide frequency ranges can be explained by simulations, as shown in Figs. 7 and 9. As discussed in Sect. 4, the uncertainty of some parameters is high. In the frequency ranges where the uncertainty of the parameters strongly influences the result, there is a wide uncertainty band in the fuzzy results. Furthermore, in some frequency ranges, there is no match between the results of the calculation methods and the measurement results, see Figs. 7b and 9b. From the results analysed here, no conclusions can be drawn about whether the measurement is influenced by factors not considered in the models or whether the measurement itself is not error-free. In view of the results, a definitive comparison of the quality of the four models used in this study is not feasible,

 Springer

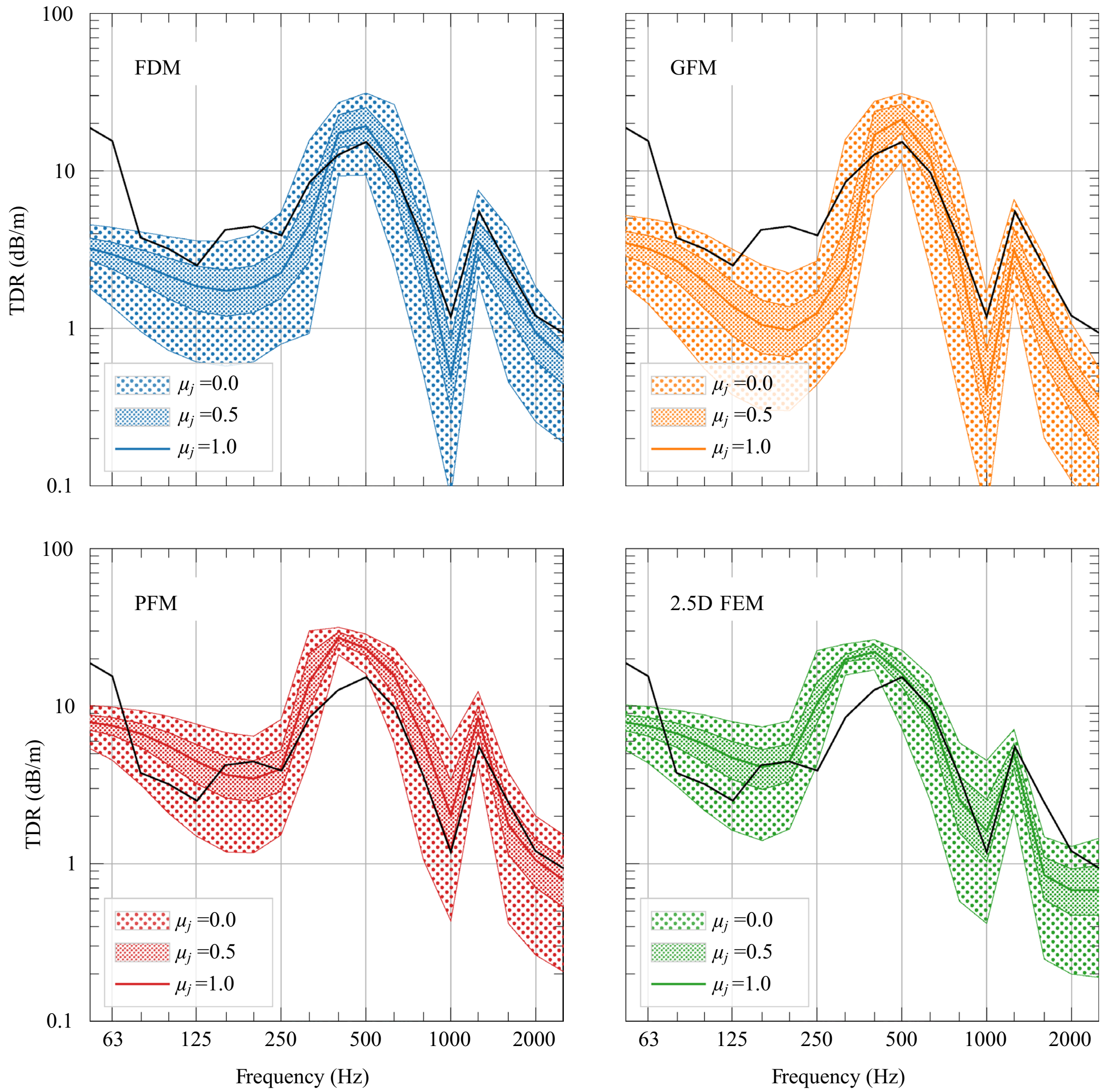

Fig. 8 Fuzzy result of TDR for the fuzzy numbers of s_p, η_p, s_b, η_b, η_r , and h_r; black line indicates the measured data

as only one measurement was considered. For example, the quality of the results in the comparison between point input mobility and TDR is very different for the four models, see Figs. 7b and 9b.

According to the literature [1], it was shown that the stiffness of the ballast in the lower frequency range and the stiffness of the pad in the higher frequency range significantly influence the point input mobility and the TDR (Figs. 10 and 11). As the uncertainty in these parameters is difficult to minimize due to the difficulty in determining the stiffness in the actual installed condition and the change with age and temperature, the influence on the results is high, it is highly recommended that these parameters be considered with the GTM for predictions. As it is difficult to determine by measurement and the influence of the loss factor of the ballast on the TDR is similar to or even more significant than the influence of the stiffness of the ballast for all four investigations, see Fig. 11, ballast damping should also be regarded as a fuzzy parameter.

Although rail wear has been shown to influence the result significantly (Fig. 5), this is often ignored in the literature. Nominal manufacturer data (see Table 3) are often used unaltered as input data for simulations [6, 21, 31], even though grinding is generally necessary before a track is used for the first time. If simulations are to be verified

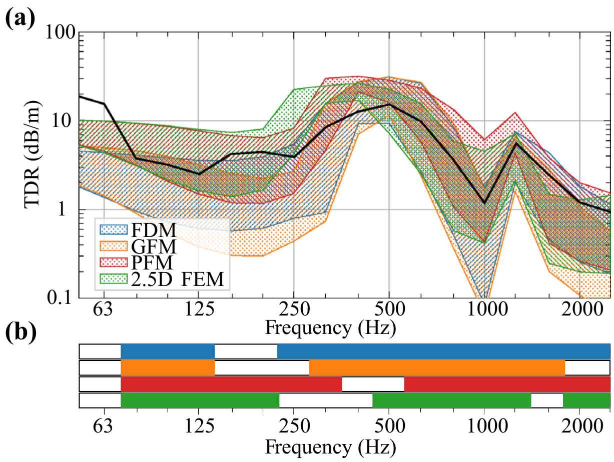

Fig. 9 Comparison of the uncertainty bands of results of TDR for the fuzzy numbers of s_p, η_p, s_b, η_b, η_r , and h_r: **a** black line indicates the measured data; **b** error of the fuzzy result, and white areas indicate that the fuzzy results cannot explain the measurement curve

with measurements, from the present results it seems to be advisable to measure the wear. For predictions in general, the wear should be considered as a fuzzy parameter.

The uncertainty of the internal damping of the rail is mainly irrelevant for calculating the point input mobility. It needs only to be considered for the TDR in the vicinity of the pinned–pinned frequency and above (Fig. 5d). The differences between the various methods are particularly obvious for η_r in the comparison between FDM and 2.5D FEM, see Fig. 11. Therefore, the need to consider rail damping as a fuzzy parameter depends on the method used.

There is no consensus in the literature regarding the use of different and method-dependent rail pad lengths in simulations. On the one hand, it is assumed that the number of support points representing the rail pad model in the longitudinal direction significantly affects the pinned-pinned mode

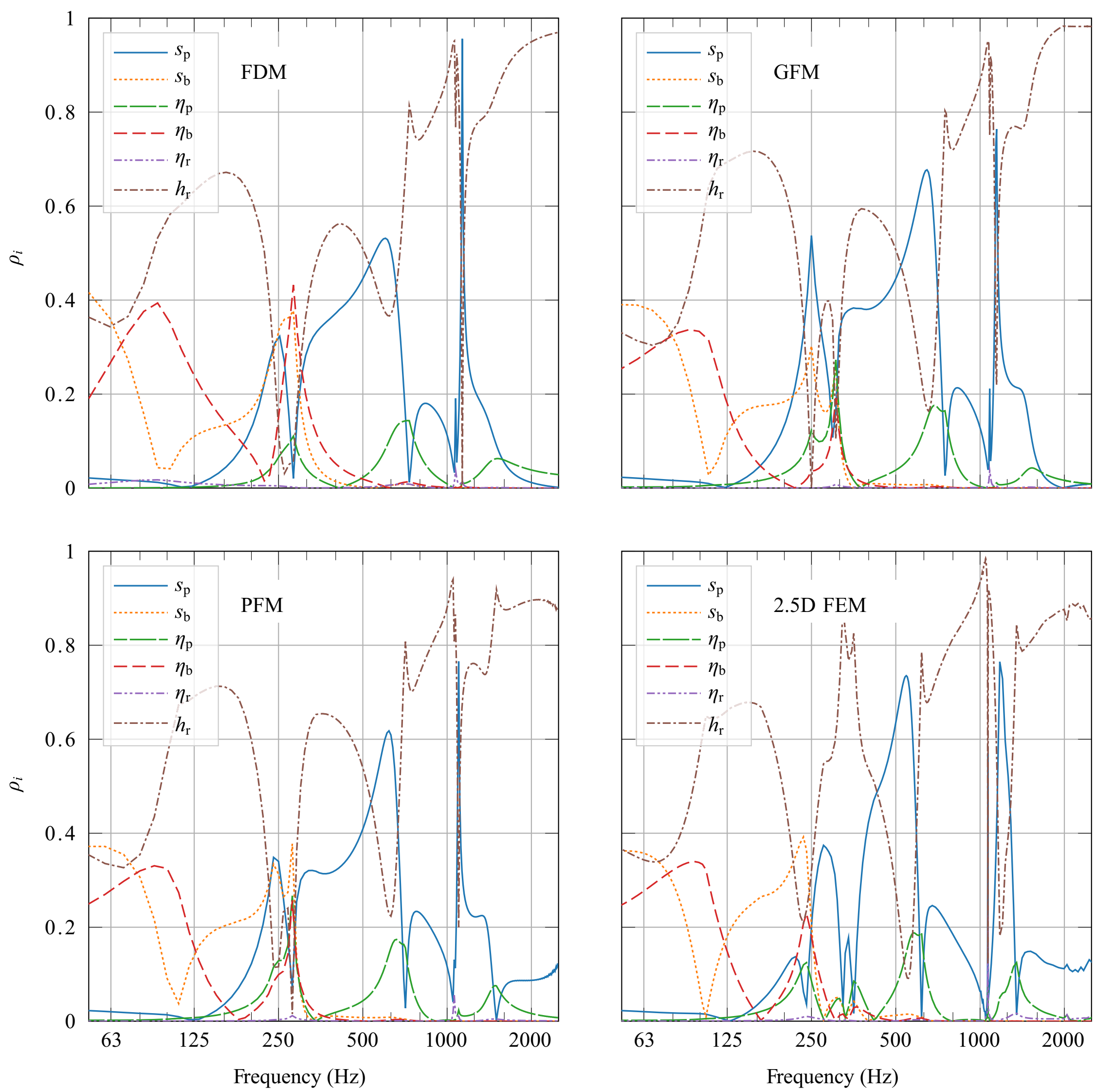

Fig. 10 Sensitivity analysis of point mobility mid-span for the fuzzy numbers of s_p, η_p, s_b, η_b, η_r , and h_r

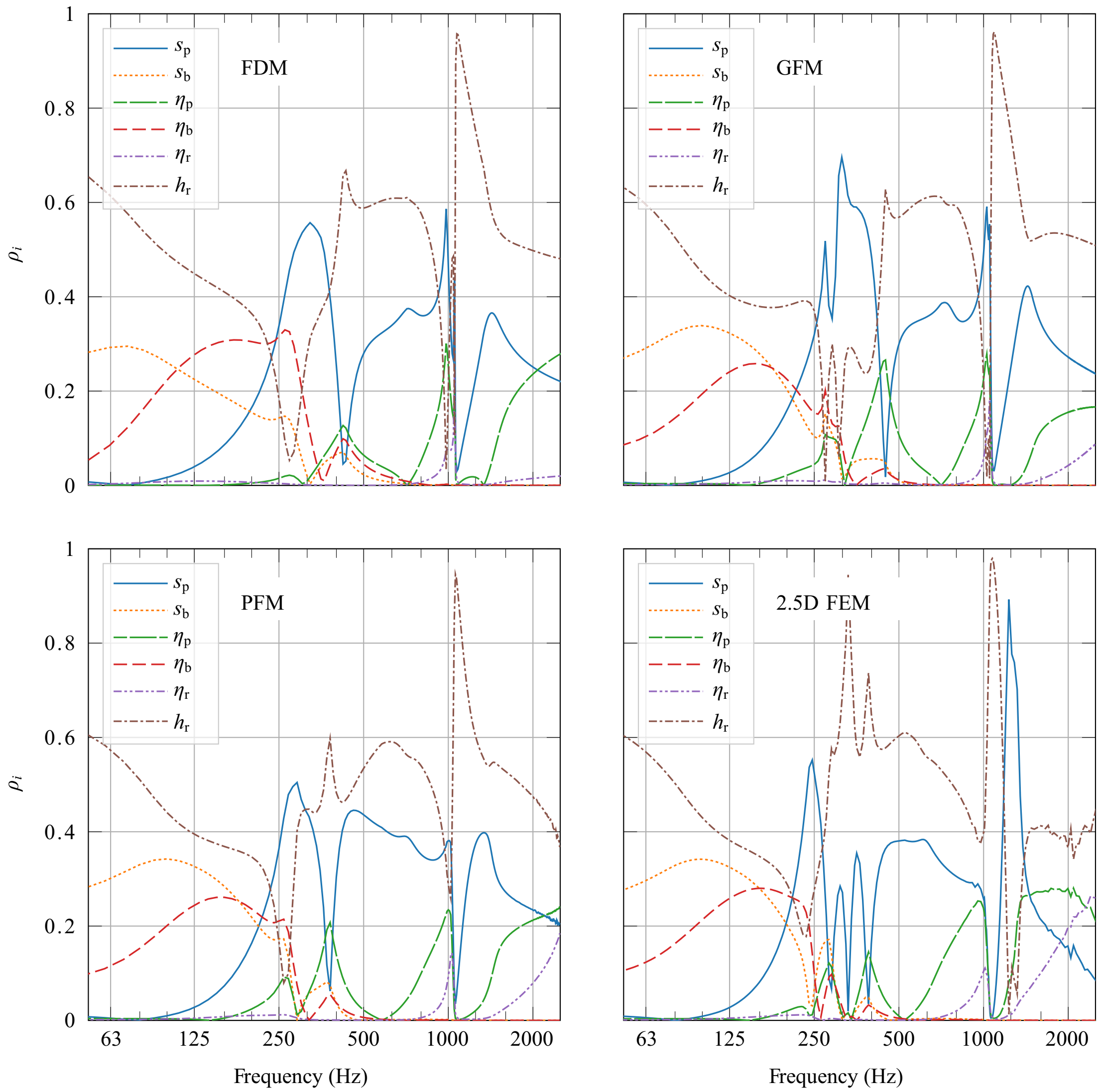

Fig. 11 Sensitivity analysis of TDR for the fuzzy numbers of s_p, η_p, s_b, η_b, η_r , and h_r

[46, 58, 59]. On the other hand, it is reported that the length of the rail pad is a less relevant parameter when the rail loss factor is higher [22]. The findings of this investigation support the assumption that the rail pad length in a longitudinal direction most significantly influences the result in the pinned–pinned frequency range after rail wear, see Fig. 12.

The parameters determined by the curve-fitting method require that the simulation curve is fitted to the point input mobility, as is often done. However, this does not necessarily give satisfactory results for the TDR. The input parameters have a different effect on the point input mobility than on the TDR. By comparing Figs. 10 and 11, it can be seen that, when considering the ballast damping for the anti-resonant frequency ω_2, the influence on the result for the TDR is more significant than when considering the point input mobility. Therefore, adjusting the parameters to the point input

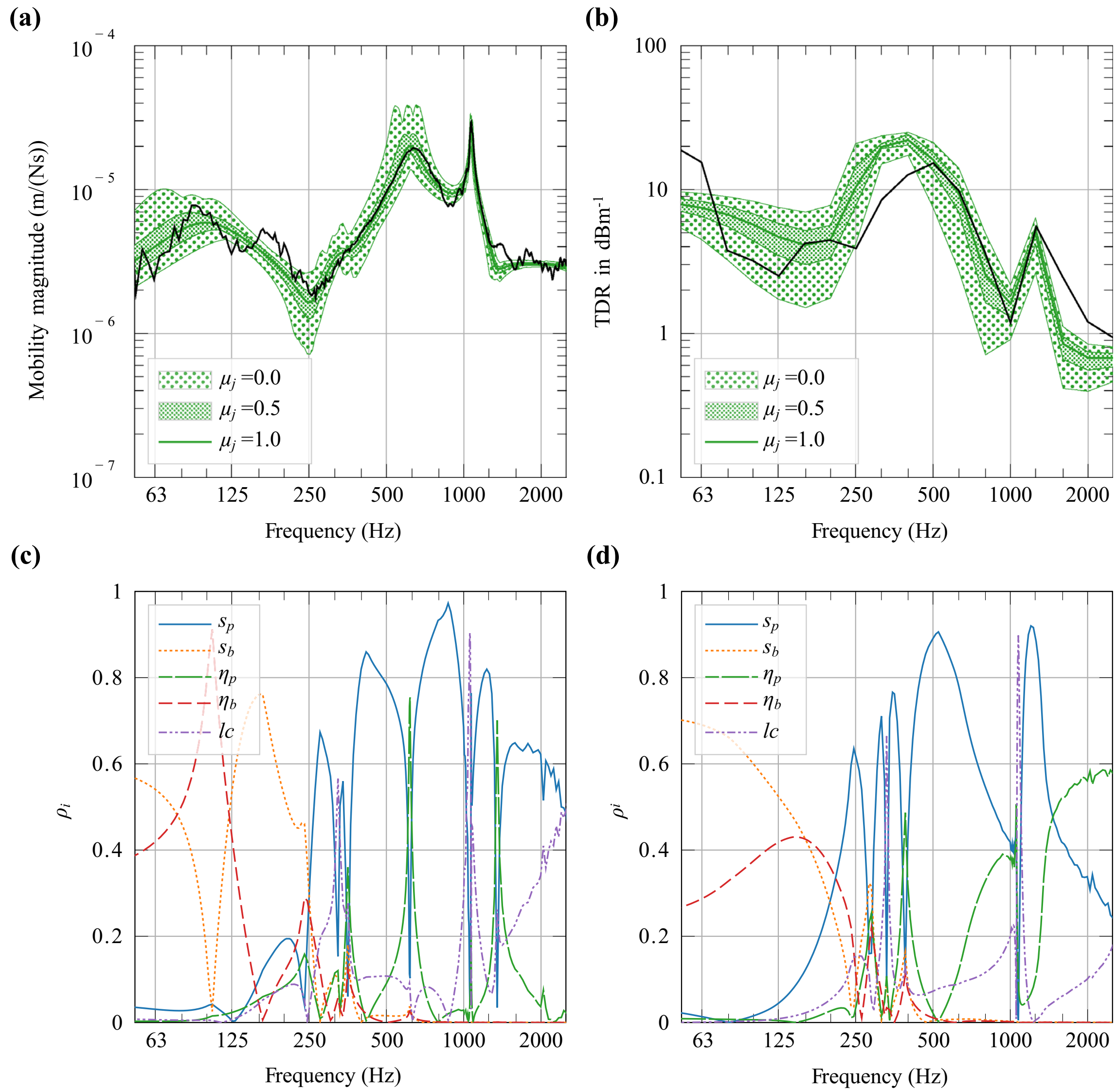

Fig. 12 Fuzzy results and sensitivity analysis of point input mobility and TDR for the fuzzy numbers of s_p, η_p, s_b, η_b , and l_c simulated with 2.5D FEM; black lines indicate the measured data: **a** point input mobility mid-span; **b** TDR; **c** degree of influence point input mobility; **d** degree of influence TDR

mobility may not be sufficient to simulate the TDR correctly, as determined for the 2.5D FEM and PFM.

8 Conclusion

The uncertainty of some input parameters required for the simulation of the dynamic track behaviour can be addressed using fuzzy arithmetic and the general transformation method. This allows to define an interval for each of the input parameters containing nominal or measured values that accounts for the uncertainty. It was demonstrated that this approach can be used for different simulation methods. As a result, frequency-dependent rail point mobilities and track decay rates were estimated as uncertainty bands. While these are assumed to contain the true results, none of the four different simulation methods considered was able to explain a set of measured results in its entirety. While this allows no definite conclusion about the four simulation methods nor about the data set, it demonstrates that the proposed approach can be used to assess the influence of uncertain input parameters in detail.

A sensitivity analysis revealed those input parameters the uncertainty of which has the largest influence on the results. While the uncertainty of the pad stiffness is often acknowledged and has a notable influence, in the present analysis it was also found that it is necessary to also pay attention to rail wear. Rail wear, which changes the mass and bending stiffness of the rail, significantly influences the results but frequently remains unconsidered. Finally, the analysis showed that the assumed contact length of the pad has a profound impact on the determination of the pinned-pinned frequency. An additional conclusion from the results is that if parameter values obtained from curve-fitting the result from one simulation method to measured results, the fitted input parameters are not well suited for the use with different methods nor to compute different dynamic track properties.

Appendix A: Conversion of loss factors to viscous damping coefficient

Several models are available for the damping in structures. The most common applied models are viscous damping and hysteretic damping. Generally, viscous damping is applicable in both the time and frequency domains. Hysteretic damping causes non-causal behaviour for simulations in the time domain and can only be used in the frequency domain. Viscous damping is described by the coefficient d. The loss factor η defines the hysteretic damping [1].

In this investigation, some models specify the damping via the loss factor. However, for the time domain method with the FDM, only the viscous damping coefficient can be considered. To use an approximately comparable damping for all models, a conversion rule is required. However, it must be pointed out that the different damping models have different properties and thus also lead to different results. Therefore, the following calculation can only be regarded as a general estimation.

The following relation between the loss factor and the viscous damping coefficient can be found [1]:

$$d = \frac{s\eta}{\omega}, \tag{12}$$

where ω is the only frequency at which both models have equal damping effect. The viscous damping increases toward high frequencies.

To ensure comparability between the frequency and time domain models, ω should match a resonant frequency since damping has the strongest influence at frequencies with the highest amplitudes [1].

However, Eq. (12) can only be used for elements specified by a stiffness, such as the pads or the ballast. No conversion is feasible for the rail with Eq. (12). Therefore, a relationship between the loss factor and the viscous damping for the rail is described here.

The equation of motion for an unsupported rail is described by Eq. (14) with a complex modulus of elasticity $E(1 + \mathrm{j}\eta_\mathrm{r})$ in the frequency domain.

$$EI_\mathrm{r}(1 + \mathrm{j}\eta_\mathrm{r})\frac{\partial^4 u}{\partial x^4} + m'_\mathrm{r}\frac{\partial^2 u}{\partial t^2} = 0 \quad , \tag{13}$$

$$EI_\mathrm{r}(1 + \mathrm{j}\eta_\mathrm{r})k^4 - m'_\mathrm{r}\omega^2 = 0 \quad . \tag{14}$$

Furthermore, the equation of motion is expressed in Eq. (16) with the viscous damping coefficient.

$$EI_\mathrm{r}\frac{\partial^4 u}{\partial x^4} + d'_\mathrm{r}\frac{\partial u}{\partial t} + m'_\mathrm{r}\frac{\partial^2 u}{\partial t^2} = 0 \tag{15}$$

$$EI_\mathrm{r}k^4 + \mathrm{j}d'_\mathrm{r}\omega - m'_\mathrm{r}\omega^2 = 0 \quad . \tag{16}$$

Compare Eqs. (14) and (16) yields

$$\begin{aligned} EI_\mathrm{r}(1 + \mathrm{j}\eta_\mathrm{r})k^4 &= EI_\mathrm{r}k^4 + \mathrm{j}d'_\mathrm{r}\omega, \\ \mathrm{j}EI_\mathrm{r}\eta_\mathrm{r}k^4 &= \mathrm{j}d'_\mathrm{r}\omega, \\ d'_\mathrm{r} &= \frac{EI\eta_\mathrm{r}k^4}{\omega}. \end{aligned} \tag{17}$$

As an approximation, the wavenumber k_b of an unsupported rail

$$k_\mathrm{b}^4 = \frac{m'_\mathrm{r}\omega^2}{EI_\mathrm{r}} \tag{18}$$

is used in Eq. (18):

$$d'_\mathrm{r} = \frac{EI_\mathrm{r}\eta_\mathrm{r}\frac{m'_\mathrm{r}\omega^2}{EI_\mathrm{r}}}{\omega} \tag{19}$$

$$= \eta_\mathrm{r}m'_\mathrm{r}\omega. \tag{20}$$

Eq. (20) approximate a relation between d'_r and η_r.

It is also reasonable to select ω so that both damping models have the same effect at the frequency with maximum deflection. In this case, the frequency ω_{c2} could be applied, as well as the pinned–pinned frequency. As the damping of the rail is especially effective in the higher frequency range, a frequency close to the pinned-pinned frequency would be appropriate (see Table 5).

Table 6 Numerical parameters for simulations with the FDM; parameters are explained in [15]

Parameter	Symbol	Value
Calculation end time	t_{end}	0.4 s
Time increment	Δt	2×10^{-5} s
Grid parameter	b	1
Local step size	Δx	0.046 m
Boundary-domain exponent	α	7
Number of boundary grid points	n_{B}	600
Force parameter	σ	0.7×10^{-10} s
Force parameter	a	0.5×10^{-2}

Appendix B: Specifications of the simulations

For the 2.5D FDM, the mesh consists of 177 nodes distributed in 36 9-node quadrilateral elements, where the typical distance between two nodes is 1.25 cm (Table 6).

References

1. Thompson DJ (2009) Railway noise and vibration: mechanisms, modelling and means of control. Elsevier, Amsterdam
2. European Committee for Standardization (2008) Railway applications-Noise emission- Characterisation of the dynamic properties of track sections for pass by noise measurements. EN 15461:2008+A1:2010
3. Lamprea-Pineda A, Connolly D, Hussein M (2021) Beams on elastic foundations-a review of railway applications and solutions. Transp Geotech 33:100696
4. Squicciarini G, Thompson DJ, Toward MGR et al (2016) The effect of temperature on railway rolling noise. Proc Inst Mech Eng Part F J Rail Rapid Transit 230(8):1777–1789
5. Federal Railroad Administration (FRA) (2015) Track inspector rail defect reference manual. Technical report, U.S. Department of Transportation, Washington DC
6. Knothe K, Grassie SL (1993) Modelling of railway track and vehicle/track interaction at high frequencies. Veh Syst Dyn 22(3–4):209–262
7. Li Q, Thompson DJ, Toward MGR (2018) Estimation of track parameters and wheel-rail combined roughness from rail vibration. Rail Rapid Transit 232(4):1149–1167
8. Gry L (1996) Dynamic modelling of railway track based on wave propagation. J Sound Vib 195(3):477–505
9. Nordborg A (1998) Vertical rail vibrations: pointforce excitation. Acta Acust Acust 84(2):280–288
10. Hanss M (2002) The transformation method for the simulation and analysis of systems with uncertain parameters. Fuzzy Sets Syst 130(3):277–289
11. Hanss M (2005) Applied fuzzy arithmetic: an introduction with engineering applications. Springer, Berlin
12. Haag T, Herrmann J, Hanss M (2010) Identification procedure for epistemic uncertainties using inverse fuzzy arithmetic. Mech Syst Signal Process 24(7):2021–2034
13. Walz NP, Hanss M (2013) Fuzzy arithmetical analysis of multibody systems with uncertainties. Arch Mech Eng 60(1):109–125
14. Seidel J, Lippert S, Estorff O (2021) Vibro-acoustical sensitivities of stiffened aircraft structures due to attached mass-spring-dampers with uncertain parameters. Aerospace 8(7):174
15. Stampka K, Sarradj E (2022) A time-domain finite-difference method for bending waves on infinite beams on an elastic foundation. Acoustics 4(4):867–884
16. Heckl MA (1995) Railway noise can random sleeper spacings help? Acta Acust Acust 81(6):559–564
17. Heckl MA (2002) Coupled waves on a periodically supported Timoshenko beam. J Sound Vib 252(5):849–882
18. Nilsson CM, Jones CJC, Thompson DJ et al (2009) A waveguide finite element and boundary element approach to calculating the sound radiated by railway and tram rails. J Sound Vib 321(3–5):813–836
19. Zhang X, Thompson DJ, Li Q et al (2019) A model of a discretely supported railway track based on a 2.5D finite element approach. J Sound Vib 438:153–174
20. Theyssen JS, Aggestam E, Zhu S et al (2021) Calibration and validation of the dynamic response of two slab track models using data from a full-scale test rig. Eng Struct 234:111980
21. Nordborg A (2002) Wheel/rail noise generation due to nonlinear effects and parametric excitation. J Acoust Soc Am 111(4):1772–1781
22. Zhang X, Thompson DJ, Jeong H (2020) Measurements of the high frequency dynamic stiffness of railway ballast and subgrade. J Sound Vib 468:115081
23. Hanss M (2000) A nearly strict fuzzy arithmetic for solving problems with uncertainties. In: 19th international conference of the North American fuzzy information processing society Atlanta, pp 439-443
24. Zadeh LA (1965) Fuzzy sets. Inf Control 8(3):338–353
25. Mantel M, Stampka K, Sarradj E (2024) Acoustic optimisation of the rail track by targeted variation of continuous superstructure parameters along the track. Acta Acustica 8(61):1–13
26. Wittel H, Muhs D, Jannasch D et al (2015) Roloff/Matek Maschinenelemente: Normung, Berechnung, Gestaltung. Springer Fachmedien Wiesbaden
27. Czichos H, Skrotzki B, Simon FG (2014) Das Ingenieurwissen: Werkstoffe. Springer, Berlin Heidelberg
28. Deutschen Institut für Normung e. V. (2017) Railway applications-Track-Rail-Part 1: Vignole railway rails 46 kg/m and above. German version EN 13674-1:2011+A1:2017
29. Deutsche Bahn AG (2011) Richtlinie 821-Oberbau inspizieren
30. Cremer L, Heckl M, Petersson BAT (2005) Structure-borne sound. Springer, Berlin, Heidelberg
31. Wu T, Thompson DJ (1999) A double Timoshenko beam model for vertical vibration analysis of railway track at high frequencies. J Sound Vib 224(2):329–348
32. Ryue J, Thompson D, White P et al (2009) Decay rates of propagating waves in railway tracks at high frequencies. J Sound Vib 320:955–976

33. Thompson DJ, Jones CJC, Wu T et al (1999) The influence of the non-linear stiffness behaviour of rail pads on the track component of rolling noise. Proc Inst Mech Eng Part F J Rail Rapid Transit 213(4):233–241
34. Wu T, Thompson DJ (1999) The effects of local preload on the foundation stiffness and vertical vibration of railway track. J Sound Vib 219(5):881–904
35. Thompson DJ, Verheij JW (1997) The dynamic behaviour of rail fasteners at high frequencies. Appl Acoust 52(1):1–17
36. Vincent N, Bouvet P, Thompson DJ et al (1996) Theoretical optimization of track components to reduce rolling noise. J Sound Vib 193(1):161–171
37. Sainz-Aja J, Carrascal I, Ferreño D et al (2020) Influence of the operational conditions on static and dynamic stiffness of rail pads. Mech Mater 148:103505
38. Thompson DJ, van Vliet WJ, Verheij JW (1998) Developments of the indirect 32 method for measuring the high frequency dynamic stiffness of resilient elements. J Sound Vib 213(1):169–188
39. Kaewunruen S, Remennikov A (2009) State dependent properties of rail pads. Technical report, University of Wollongong Research Online
40. Huber P, Schneider P (2021) Forschungsprojekt Schienenbefestigung Phase “I”. Schlussbericht version 1.2, KPZ Fahrbahn
41. Hasap A, Noraphaiphipaksa N, Kanchanomai C (2020) Influence of malposition on the performance of elastic rail clip: Toe load, stress, and friction. Structures 28:2661–2670
42. Oregui M, Núñez A, Dollevoet R et al (2017) Sensitivity analysis of railpad parameters on vertical railway track dynamics. J Eng Mech 143(5):04017011
43. Fenander Å (1997) Frequency dependent stiffness and damping of railpads. Proc Inst Mech Eng Part F J Rail Rapid Transit 211(1):51–62
44. Thompson DJ, Jones C (1999) The effects of rail support stiffness on railway rolling noise. J Acoust Soc Am 105:947–947
45. Oscarsson J (2002) Simulation of train-track interaction with stochastic track properties. Veh Syst Dyn 37(6):449–469
46. Ferrara R, Leonardi G, Jourdan F (2013) A contact-area model for rail-pads connections in 2-D simulations: sensitivity analysis of train-induced vibrations. Veh Syst Dyn 51(9):1342–1362
47. Heinrich Krug GmbH & Co. KG (2016) Zwischenlagen (pads) https://www.heinrich-krug.de/oberbau/zwischenlagen/. Accessed 5 May 2024
48. Kostovasilis D, Thompson DJ, Hussein MFM (2017) A semi-analytical beam model for the vibration of railway tracks. J Sound Vib 393:321–337
49. Zhai W, Wang K, Lin J (2004) Modelling and experiment of railway ballast vibrations. J Sound Vib 270(4):673–683
50. Sadri M, Steenbergen M (2018) Effects of railway track design on the expected degradation: parametric study on energy dissipation. J Sound Vib 419:281–301
51. Walton-Macaulay C, Bryson LS, Guenther KJ (2014) Experimental study on the stiffness degradation of railroad ballast subjected to clay fouling. In: 2014 Joint Rail Conference, Colorado Springs, pp V001T01A004
52. Kaewunruen S, Ngamkhanong C, Ng J (2019) Influence of time-dependent material degradation on life cycle serviceability of interspersed railway tracks due to moving train loads. Eng Struct 199:109625
53. Deutschen Institut für Normung e. V. (2016) Railway applications-Concrete sleepers and bearers-Part 1: general requirements. German version EN 13230-1:2016
54. Shenton MJ (1978) Deformation of railway ballast under repeated loading conditions. In: Railroad Track Mechanics and Technology, Proceedings of a Symposium Held at Princeton University, Princeton, pp 405–425
55. Gourley T (1996) Concrete railway sleeper durability. In: Eleventh International Rail Track Conference. Adelaide, pp 143–150
56. Li Q, Thompson DJ, Toward M (2017) Dataset for paper: estimation of track parameters and wheel-rail combined roughness from rail vibration. University of Southampton. https://doi.org/10.5258/SOTON/D0068
57. Dlubal Software GmbH. Querschnittswerte UIC (abgenutzt) Standardquerschnitte der Deutschen Bahn, abgenutzt. https://www.dlubal.com/de/ querschnittswerte/series-uic-abgenutzt-din-en-13674-1. Accessed May 5 2023
58. Mazilu T, Leu M (2017) Impact of the rail-pad multi-discrete model upon the prediction of the rail response. IOP Conf Ser: Mater Sci Eng 227:012079
59. Blanco B, Alonso A, Kari L (2018) Distributed support modelling for vertical track dynamic analysis. Veh Syst Dyn 56(4):529–552